Research Article Vol. 5, No. 5 / May 2018 / Optica 564

Monolithically integrated InGaN/GaN light-emitting diodes, photodetectors, and waveguides on Si substrate

K. H. Li,[1] W. Y. Fu,[1] Y. F. Cheung,[1] K. K. Y. Wong,[1] Y. Wang,[2] K. M. Lau,[3] and H. W. Choi[1,*]

[1]Department of Electrical and Electronic Engineering, The University of Hong Kong, Hong Kong, China
[2]Grünberg Research Centre, Nanjing University of Posts and Telecommunications, Nanjing 210003, China
[3]Department of Electronic and Computer Engineering, Hong Kong University of Science and Technology, Hong Kong, China
*Corresponding author: hwchoi@hku.hk

Received 22 January 2018; revised 6 April 2018; accepted 10 April 2018 (Doc. ID 320413); published 8 May 2018

The characteristics of monolithically integrated light-emitting diodes (LEDs), photodetectors (PDs), and waveguides on a GaN-on-Si wafer are investigated. The InGaN/GaN multi-quantum wells, which are responsible for blue light emission in LEDs, are also used for photodetection in PDs. Despite the Stokes shift, a spectral overlap of ~25 nm between the emission and absorption spectra provides the PDs with sufficient photosensitivity to signals from the emitter while remaining insensitive to ambient lighting. Optical interconnects in the form of linear or bent suspended waveguides bridging the LEDs and PDs are formed by selective detachment of etched GaN mesas from the Si substrate. Additionally, the PDs can be detached from the substrate and remounted on an elevated platform, owing to the flexibility of the thin-film waveguide. The 150 μm × 150 μm LEDs and PDs exhibit rapid response on nanosecond time scales, which is attributed to fast radiative recombinations as well as minimized resistive-capacitive (RC) delays, enabling transmission of pseudorandom binary sequence (PRBS) data signals at rates of 250 Mb/s with an opening in the eye diagram. Together with multichannel transmission free of crosstalk, the ability of the planar and three-dimensional monolithic photonic systems to handle visible-light communication (VLC) applications is demonstrated.

OCIS codes: (220.0220) Optical design and fabrication; (230.0230) Optical devices; (230.3120) Integrated optics devices; (250.5300) Photonic integrated circuits.

https://doi.org/10.1364/OPTICA.5.000564

1. INTRODUCTION

Similar to the trend of Si-based electronic integrated circuits, the monolithic integration of vast numbers of different photonic components on a single chip is of paramount importance in the drive to enhance system functionality, speeds, efficiencies, and robustness. In the GaN-based family of devices, many of these devices have become very successful commercial products, including light-emitting diodes (LEDs) for lighting, laser diodes (LDs) for optical storage, and high-electron-mobility transistors (HEMTs) for power electronics [1–3]. Additionally, GaN-based photodetectors (PDs) and microelectromechanical systems (MEMS) are also finding their niche in specific detection and sensing applications [4,5]. The ability to integrate all of these components onto a single platform would render powerful systems such as lab-on-a-chip devices and photonic integrated circuits (PICs) for various applications. However, such ambitious goals are hindered by incompatibilities between the structures of different devices, as well as processing constraints. Nevertheless, the integration of light-related components is realistic in view of their inherent similarities. InGaN/GaN light-emitters based on multi-quantum-wells (MQWs) are ideal candidates for visible light communication (VLC) applications due to their attractive properties, which include high quantum efficiencies and rapid time responses [6,7]. For on-chip communications, a photodetector that can detect light emitted by the MQWs must be integrated onto the same wafer. Also, given the omnidirectional nature of LED emission, free-space transmission is not practical. Instead, waveguides must be integrated to efficiently route optical signals. Recently, the monolithic integration of transmitters, waveguides, and receivers on the GaN-on-Si platform for in-plane data transmission at up to 120 Mb/s [8,9] has been demonstrated. However, the characteristics of such systems have not been investigated, particularly the spectral sensitivity of the MQW detector and the temporal responses of the transmitters and receivers, as well as the optical coupling and transmission of the etched waveguides. In this work, a detailed investigation has been done to

gain a deeper understanding of the mechanisms and limitations of the emission, transmission, and absorption processes in such monolithic systems.

A GaN-on-Si platform for the integration of LEDs, PDs, and waveguides on a single chip is schematically illustrated in Fig. 1(a). The MQWs, which are responsible for light emission in the LEDs, absorb light emitted by the LEDs to generate electrical signals. Transparent GaN-suspended waveguides are formed by selectively separating dry-etched GaN mesas from the Si substrate using a selective wet etch process. The electrical and optical properties of the individual components are comprehensively characterized, followed by an investigation of the performance of the overall system and its different components. In addition to conventional two-dimensional (2D) photonic systems of planar configurations, a 3D structure is also assembled by mounting a detached PD onto an elevated platform, with the bent waveguide functioning as an optical fiber for signal routing between two horizontal planes. While high-speed, on-chip visible light communication (VLC) in the planar and 3D photonic systems is demonstrated in this work, the platform can be further extended to applications such as on-chip intensity monitoring of LEDs and lab-on-a-chip devices [10–12].

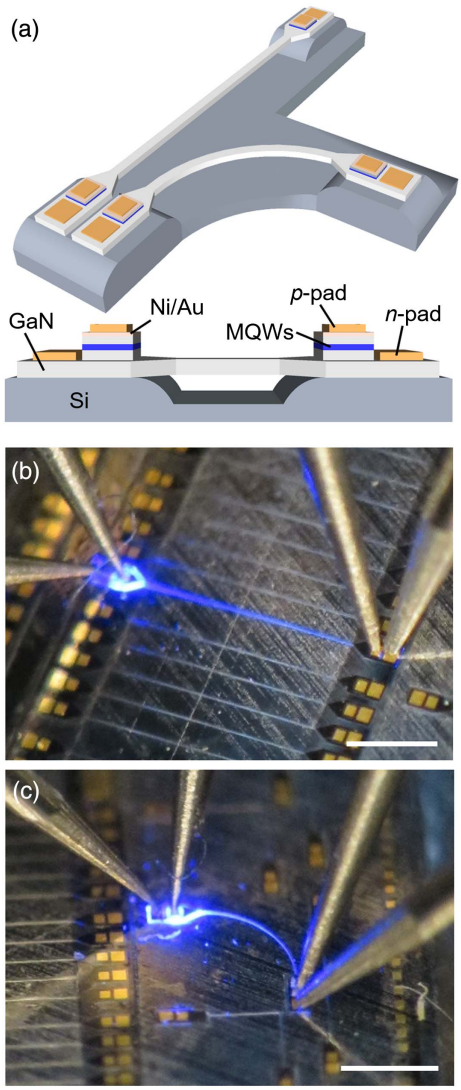

Fig. 1. (a) Schematic diagrams illustrate the integration of LEDs, PDs, and waveguides on a GaN-on-Si wafer. Microphotographs show optical transmission between LEDs and PDs connected between (b) linear and (c) bent waveguides. The scale bars in (b) and (c) represent 1 mm in length.

2. EXPERIMENTAL DETAILS

The blue-light-emitting LED wafer is grown by metal–organic chemical vapor deposition (MOCVD) on a six-inch Si substrate. The epitaxial structure consists of a 1.2 μm thick graded AlGaN buffer, a 0.57 μm thick undoped GaN layer, a 2.1 μm thick n-type GaN layer, 10 pairs of InGaN/GaN MQWs with a total thickness of 0.14 μm, and a 0.15 μm thick p-type GaN layer. A Ni/Au (5 nm/5 nm) current spreading layer is deposited onto the p-GaN layer by electron beam (e-beam) evaporation, followed by rapid thermal annealing (RTA) in an oxygen ambient. The mesas of the LED and the PD with identical dimensions of 150 μm × 150 μm are patterned by photolithography followed by Cl_2-based inductively coupled plasma (ICP) etching down to the n-GaN layer, removing the p-GaN and MQWs layers. A 1.5 μm thick SiO_2 layer is deposited by plasma-enhanced chemical vapor deposition. A 30 μm wide waveguide pattern interconnecting the LED and the PD is defined by photolithography and transferred onto the SiO_2 layer by SF_6-based ICP etching, which in turn serves as a hard mask for pattern transfer onto GaN by Cl_2-based ICP etching down to the Si substrate. The p-pads and n-pads are e-beam evaporated, followed by RTA. The Si beneath the waveguide is selectively wet etched using an HF/HNO_3 mixture to form the suspended structure. The schematic diagram in Fig. 1(a) shows a representative section of the system, while the microphotographs in Figs. 1(b) and 1(c) illustrate optical transmission between the LEDs and PDs connected by linear and bent waveguides, respectively, demonstrating the versatility of optical signal routing.

3. RESULTS AND DISCUSSION

Figure 2 shows the EL spectrum of the LED operated at 1 mA, whose center wavelength and spectral width (FWHM) are evaluated to be ~452 nm and ~23 nm, respectively. Since the MQW structure is intended for light emission, its ability to detect light emitted by itself is particularly critical to determine the system's functionality, which is dependent on the Stokes shift between the absorption and emission processes. Detection sensitivity will drop to zero if the absorption edge shifts beyond the emission spectra.

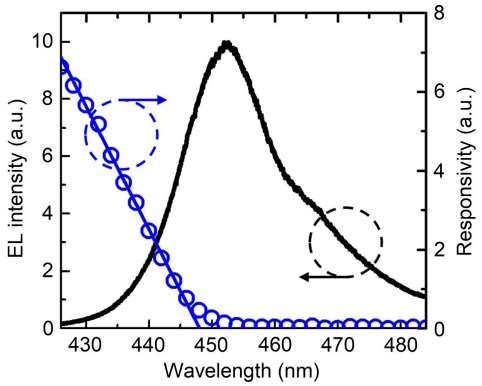

Fig. 2. EL spectrum of the LED operated at 1 mA and spectral responsivity of the PD.

The Stokes shift can be approximated as the exciton binding energy because this amount of energy is required to combine an electron and a hole to emit a photon at a lower energy. According to calculations by Wei *et al.* [13], the *maximum* exciton binding energy in blue-light-emitting QWs (of less than 20% In content) is ~58.1 meV, which corresponds to an absorption edge at 442.6 nm for our MQWs with an emission peak at 452 nm, suggesting that using the MQWs as PDs to detect MQW emission is feasible. To verify this assumption, the spectral responsivity of the MQW PD is measured by irradiating the device with monochromatic light generated from a broadband light source dispersed through a monochromator (Acton SP2500A) and plotted with the emission spectrum in Fig. 2. The absorption edge is determined to be ~447.7 nm, while band-tailing effects due to In content fluctuations in the wells extend the responsivity to ~452 nm, which corresponds to the emission peak wavelength, effectively providing ~25 nm of overlap between the emission and absorption spectra.

Having verified the feasibility of using the MQWs for detection, an effective means of optical transmission between the emitters and detectors must be established. Unlike electronic systems where electrical signals are readily routed via metallic interconnects, optical signal transmission is more complicated. For free-space transmission in photonic systems, the optical signals from the emitters must be directed to the detectors with high precision. This transmission requires arrays of miniature laser diodes with high pointing accuracies and stabilities, which is challenging. The use of external waveguides typically constructed from polymeric materials with highly dissimilar refractive indices requires careful alignment, which may limit optical coupling and confinement. In this work, the optical signals are routed using waveguides formed on the same epitaxial layer as the LEDs and PDs, thereby optimizing the coupling of lateral propagating light from the MQW into the waveguide. As demonstrated in Figs. 1(b) and 1(c), the waveguides are not restricted to linear geometries. Instead, freeform waveguides can readily be implemented as optical links between non-line-of-sight (NLOS) components. Despite the use of incoherent sources, optical coupling losses are minimized because the waveguides are physically attached to the emitters and detectors.

Optical transmission across the GaN waveguides is studied by optical ray tracing. Figure 3(a) illustrates the propagation of optical rays along a GaN-on-Si waveguide of 4 μm × 30 μm × 1 mm. It is observed that the downward propagating rays are readily absorbed by the Si substrate, resulting in an optical transmittance (defined as the ratio of transmitted optical power to incident optical power) of 2.2%. For comparison, the simulations are repeated for a waveguide of identical dimensions formed on sapphire, another common substrate for GaN, as shown in Fig. 3(b). With a refractive index contrast of ~0.7 (at 460 nm) between GaN and sapphire, the optical transmittance is increased to 56.4%. The highest refractive index contrast is provided by air as a surrounding medium. Previously, suspended GaN-on-Si microdisks have been demonstrated using a selective wet etch process [14]. The same technique is applied to form suspended waveguides by selectively removing Si beneath the GaN waveguides to maximize optical confinement. Simulations, depicted in Fig. 3(c), predict optical transmittance of 73.8%, a marked improvement over the waveguides attached to either substrate. Optical transmission in the suspended waveguides as a function of transmission distance is ray-trace simulated and plotted in Fig. 3(d), from which an exponential decay constant of ~0.13 cm^{-1} is determined. The optical transmission properties of the waveguides are also determined experimentally by coupling a 405 nm laser beam through an objective lens onto the waveguide at normal incidence. The measured photocurrents as functions of transmission distances are also plotted in Fig. 3(d), which exhibits exponential decay characteristics with a decay constant of ~0.74 cm^{-1}.

The experimentally determined decay constant is found to be ~5.7 times higher than the simulated value, due to the

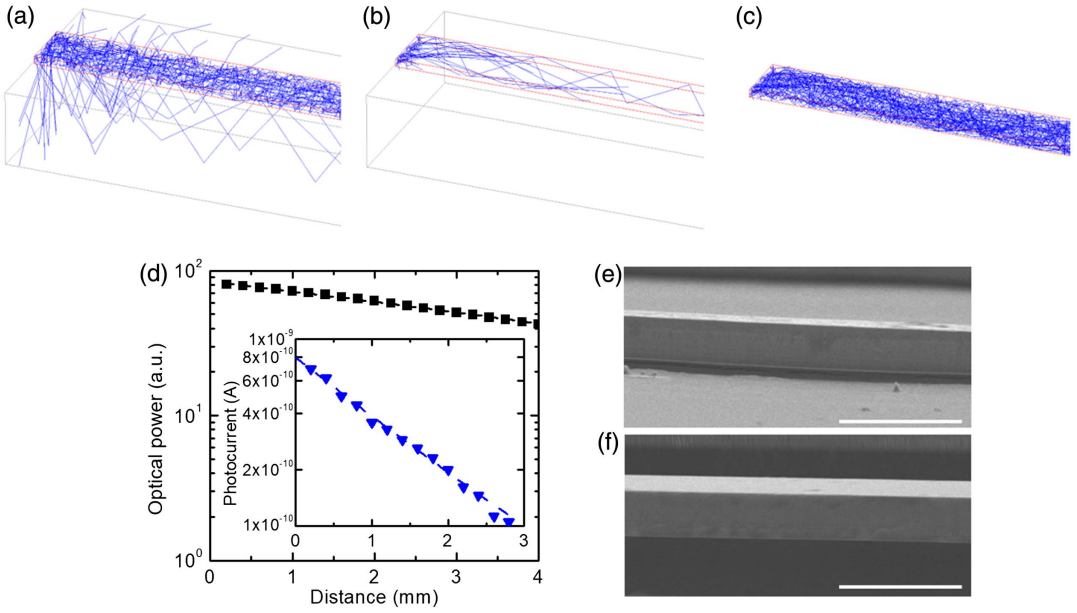

Fig. 3. Ray-trace simulation results of the (a) GaN-on-sapphire (b) GaN-on-Si, and (c) suspended waveguides. (d) Simulated optical power in the suspended waveguides as a function of distance. The set shows PD photocurrent as a function of the laser irradiation position. SEM (top oblique view) images show the waveguide morphologies. (e) Before and (f) after wet etching. The scale bars represent 10 μm in length.

assumption of ideally smooth optical surfaces in the ray-trace simulations. However, surface roughness may be sustained during the fabrication process, which involves plasma and wet etching. The scanning electron microscope (SEM) images in Figs. 3(e) and 3(f) show the waveguides before and after wet etching, respectively. The morphologies of the top and bottom surfaces of the waveguides are further evaluated by atomic force microscopy (AFM), from which optically smooth root-mean-square (rms) roughness of 3.3 nm ($\sim\lambda/130$) and 1.8 nm ($\sim\lambda/235$) have been determined, respectively. The major source of optical loss may thus be attributed to scattering caused by roughness on the vertical sidewalls of the waveguide, a consequence of mask erosion and/or ion-induced damage during plasma etching [15,16].

The electrical responses of the PDs are determined by measuring the photocurrents as functions of voltages at different levels of illumination intensity from the LED. As plotted in Fig. 4(a), the dark currents measured under reverse bias voltages are within the range of 1–10 pA, rising by more than three orders of magnitude to 19–290 nA when the LEDs are driven at 1 to 20 mA. The photocurrents are also found to increase linearly with LED injection currents. The photocurrents are also measured under ambient lighting conditions without biasing the LED emitters. As shown in the I-V plot of Fig. 4(b), the photocurrent levels under ambient lighting are identical to those of dark currents, implying that the system will not be sensitive to lighting conditions in the environment, made possible by metallic coverage over the PD. Optical transmission along the 2.4 mm long waveguides are also demonstrated to be free of crosstalk, since individual photocurrents are unaffected by optical transmission along adjacent channels with separations of 240 μm, as shown in Fig. 4(b). In addition, the I_{PD} – V characteristics of 1.5 mm long bent waveguides have been measured and compared with linear waveguides of identical lengths, as plotted in Fig. 4(c). The photocurrents of the bent waveguides are reduced by ∼5.7 times due to bending losses.

The operational bandwidth of a communication system is fundamentally limited by the frequency responses of the light sources and detectors. It is known that the InGaN/GaN QWs exhibit rapid radiative recombination rates on the nanosecond time scale [17,18]; as such, InGaN/GaN LEDs are ideally suited as high-speed emitters. From the time-resolved photoluminescence (PL) spectrum plotted in Fig. 5(a), an exponential decay time constant t_{TRPL} of ∼1.8 ns is obtained. For photoelectric conversion in LEDs and PDs, an additional resistive-capacitive (RC) decay limits the system response. One of the most direct and effective approach to accelerate device response is a corresponding reduction in device dimensions. The LED emitters are thus designed to be tens of microns in size to minimize the RC time constant t_{RC}, as well as to facilitate component integration on a larger scale. With a capacitance of ∼8 pF obtained from capacitance-voltage (C-V) measurements and a combined series and load resistance of 76 Ω as determined from current–voltage (I-V) measurements, t_{RC} is evaluated as 0.64 ns. By injecting a short electrical pulse (8 ns pulse width, 50% duty cycle) to the LED, the transient response of the PD is measured and plotted in Fig. 5(b), from which rise and fall times are determined to be 1.1 ns and 2.0 ns, respectively, which are close to t_{TRPL} and t_{RC}, suggesting that the dimensions of the devices have been optimized.

With rapid responses, the LED–waveguide–PD combinations are well suited for high-speed signal transmission. To demonstrate such capabilities, an on-chip visible light communication (VLC) system is constructed, as depicted in Fig. 5(c). A data signal in the form of a pseudorandom binary sequence (PRBS) with a peak-to-peak of 0.5 V and a pattern length of $2^{17} - 1$ is generated by an arbitrary waveform generator (AWG). The PRBS signal is amplified and dc-biased with a bias tee to obtain a voltage swing from 0 to 7 V. The fast-responding LED converts the electrical PRBS signal into optical pulses, which transmit down the waveguide for absorption by the PD. The generated photocurrent is amplified by a transimpedance amplifier (TIA) and analyzed by an oscilloscope synchronized with the AWG. At a data bit rate of 250 Mbit/s, a clear opening is observed in the eye diagram of Fig. 5(d), demonstrating the potential for high-speed VLC applications. The system speeds can readily be boosted by applying modulation schemes such as orthogonal frequency-division multiplexing (OFDM) [19].

While planar optical transmission between NLOS components has been demonstrated, nonplanar signal transmission will not be possible due to the rigidity of the waveguides. 3D integration is becoming increasingly popular owing to the reduced form factor, density multiplication, and improved performance. For electrical 3D systems, the vertically bonded chips can be interconnected by through silicon via (TSV) [20]. Flexible waveguides may be the solution for optical 3D systems, coupling optical

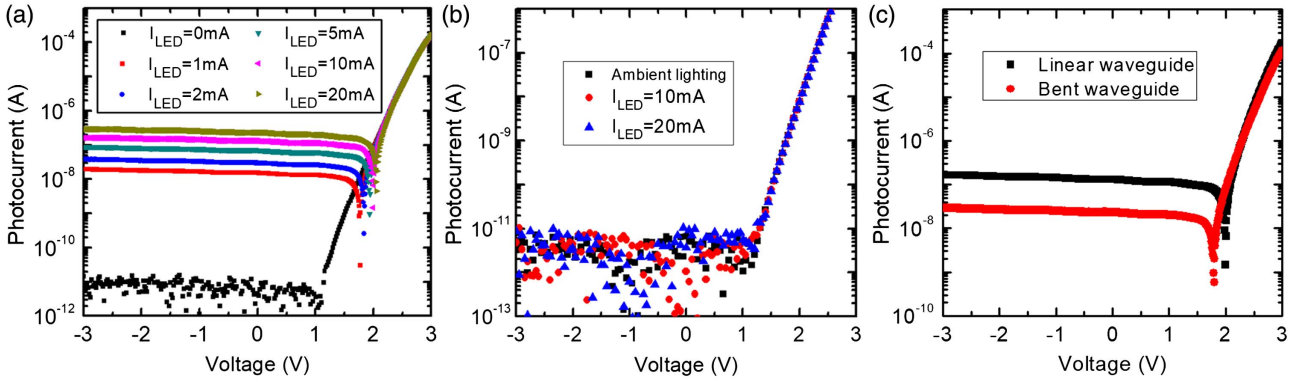

Fig. 4. (a) I_{PD} – V plots of the PD responding to illumination from the LED operated at currents from 0 (dark) to 20 mA. (b) I_{PD} – V plots of the PD under ambient lighting conditions and optical transmission in an adjacent channel. (c) I_{PD} – V characteristics of planar systems with linear and bent waveguides.

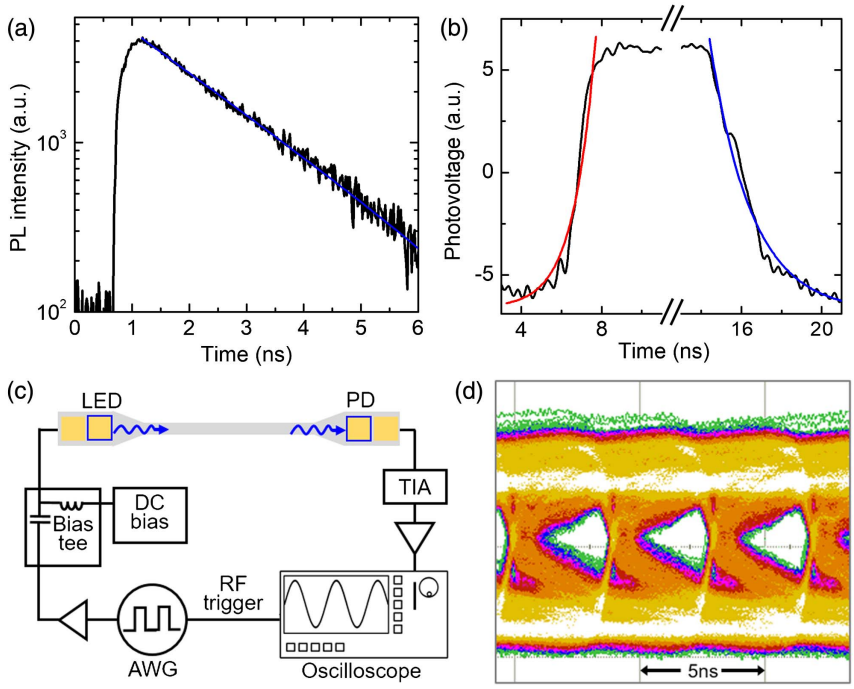

Fig. 5. (a) Time-resolved PL decay curve of the InGaN/GaN QWs structure measured at room temperature. (b) Transient photocurrent response of the PD when driven by a short pulse. The red and blue lines represent the rising and falling edges, respectively. (c) Schematic diagram of the experimental setup for evaluating data transmission performance. (d) Measured eye diagram of transmission of a PRBS signal at 250 Mb/s.

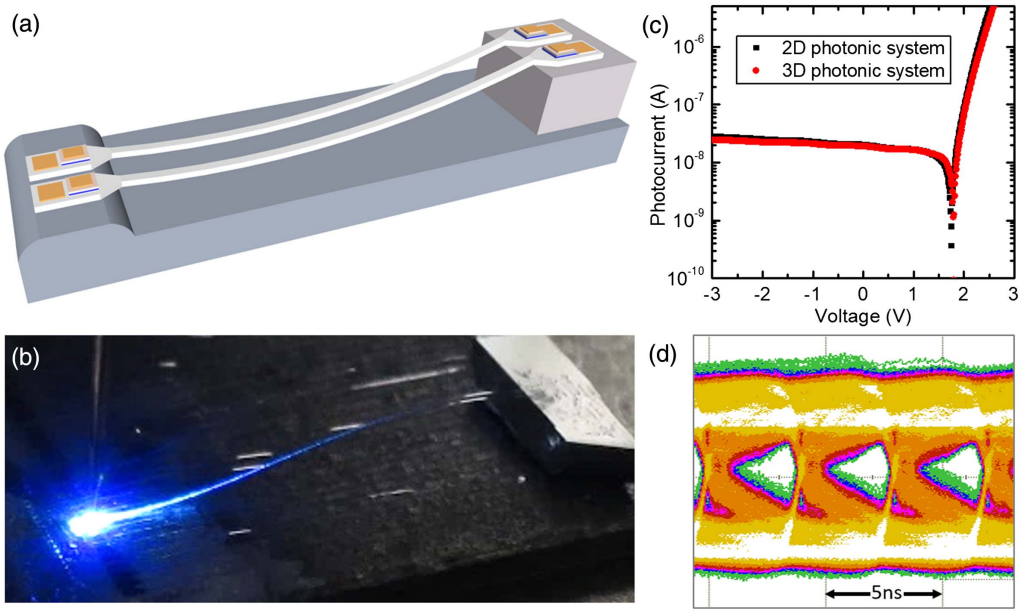

Fig. 6. (a) Schematic diagram and (b) microphotograph of the 3D photonic system. (c) I_{PD} – V plots of the PDs before and after selective-area liftoff. (d) Measured eye diagram of transmission of a PRBS signal at 250 Mb/s in the 3D photonic system.

signals, as illustrated in the schematic diagram of Fig. 6(a). To achieve this solution, the Si beneath both the waveguide and the PD are simultaneously removed by selective area wet etching. A detailed description of the process is provided in Supplement 1. After etching, both the 10 mm long and 50 μm wide waveguides and the PD become suspended to form a flexible structure while the LED remains attached to the Si substrate. The suspended PD is bonded onto a Si block to emulate a 3D photonic system, as shown in the photograph of Fig. 6(b). A reduction in the photocurrent of ∼12% is observed due to losses in the mildly bended flexible waveguide, as illustrated in Fig. 6(c). Like the 2D photonic system, the 3D system can transmit a PRBS signal at a data bit rate of 250 Mb/s, which is evident from the eye diagram shown in Fig. 6(d).

4. CONCLUSION

In summary, LEDs, PDs, and waveguides have been fabricated onto the same GaN-on-Si wafer containing InGaN/GaN MQWs. The MQWs simultaneously act as light emitters and detectors in the LEDs and PDs, respectively, while the waveguides are constructed from the GaN layers. The photosensitivity of the MQW PDs is investigated; a spectral overlap of ~25 nm enables the PDs to detect light emitted by the LEDs using identical MQWs. The LEDs and PDs are air-bridged with suspended GaN waveguides with high optical confinement, formed by selective removal of the Si substrate underneath the waveguides. Fast radiative recombination lifetimes, together with low RC delays, result in device transient responses of a few nanoseconds. Apart from linear and bent waveguides, flexible thin-film waveguides formed by detachment of the PD and remounted onto an elevated platform demonstrate the feasibility of optical signal routing in multilevel 3D photonic systems. With PRBS transmission rates of up to 250 Mb/s, the planar and 3D photonic systems serve as proof-of-concept platforms for on-chip VLC applications.

Funding. Research Grants Council, University Grants Committee (RGC, UGC) (N_HKU710/15, T23-612/12-R); National Natural Science Foundation of China (NSFC).

Acknowledgment. The work described in this paper was jointly supported by grants from the NFSC/RGC Joint Research Scheme sponsored by the RGC of Hong Kong and the National Natural Science Foundation of China and the Theme-based Research Scheme sponsored by the RGC of Hong Kong.

See Supplement 1 for supporting content.

REFERENCES

1. M. Razeghi, "III-nitride optoelectronic devices: from ultraviolet toward terahertz," IEEE Photon. J. **3**, 263–267 (2011).
2. J. W. Orton and C. T. Foxon, "Group III nitride semiconductors for short wavelength light-emitting devices," Rep. Prog. Phys. **61**, 1–75 (1998).
3. U. K. Mishra, L. Shen, T. E. Kazior, and Y. F. Wu, "GaN-based RF power devices and amplifiers," Proc. IEEE **96**, 287–305 (2008).
4. E. Munoz, E. Monroy, J. L. Pau, F. Calle, F. Omnes, and P. Gibart, "III nitrides and UV detection," J. Phys. **13**, 7115 (2001).
5. V. Cimalla, J. Pezoldt, and O. Ambacher, "Group III nitride and SiC based MEMS and NEMS: materials properties, technology and applications," J. Phys. D **40**, 6386–6434 (2007).
6. S. Nakamura, N. Senoh, N. Iwasa, and S. I. Nagahama, "High-brightness InGaN blue, green and yellow light-emitting-diodes with quantum-well structures," Jpn. J. Appl. Phys. **34**, L797–L799 (1995).
7. J. J. D. McKendry, R. P. Green, A. E. Kelly, Z. Gong, B. Guilhabert, D. Massoubre, E. D. Gu, and M. D. Dawson, "High-speed visible light communications using individual pixels in a micro light-emitting diode array," IEEE Photon. Technol. Lett. **22**, 1346–1348 (2010).
8. J. L. Yuan, X. M. Gao, Y. C. Yang, G. X. Zhu, W. Yuan, H. W. Choi, Z. Y. Zhang, and Y. J. Wang, "GaN directional couplers for on-chip optical interconnect," Semicond. Sci. Technol. **32**, 045001 (2017).
9. Z. Shi, X. Gao, J. Yuan, S. Zhang, Y. Jiang, F. Zhang, Y. Jiang, H. Zhu, and Y. Wang, "Transferrable monolithic III-nitride photonic circuit for multifunctional optoelectronics," Appl. Phys. Lett. **111**, 241104 (2017).
10. H. W. Choi, K. H. Li, and H. Lu, "Light-emitting diodes (leds) with monolithically-integrated photodetectors for in situ real-time intensity monitoring," WO Application WO2017197576A1 (November 23, 2017).
11. M. C. Estevez, M. Alvarez, and L. M. Lechuga, "Integrated optical devices for lab-on-a-chip biosensing applications," Laser Photon. Rev. **6**, 463–487 (2012).
12. A. L. Washburn and R. C. Bailey, "Photonics-on-a-chip: recent advances in integrated waveguides as enabling detection elements for real-world, lab-on-a-chip biosensing applications," Analyst **136**, 227–236 (2011).
13. S. Y. Wei, Y. L. Jia, and C. X. Xia, "Excitonic optical absorption in wurtzite InGaN/GaN quantum wells," Superlatt. Microstruct. **51**, 9–15 (2012).
14. H. W. Choi, K. N. Hui, P. T. Lai, P. Chen, X. H. Zhang, S. Tripathy, J. H. Teng, and S. J. Chua, "Lasing in GaN microdisks pivoted on Si," Appl. Phys. Lett. **89**, 211101 (2006).
15. P. Frajtag, N. A. El-Masry, N. Nepal, and S. M. Bedair, "Embedded voids approach for low defect density in epitaxial GaN films," Appl. Phys. Lett. **98**, 023115 (2011).
16. Y. Y. Zhang, Z. T. Ma, X. H. Zhang, T. Wang, and H. W. Choi, "Optically pumped whispering-gallery mode lasing from 2-μm GaN micro-disks pivoted on Si," Appl. Phys. Lett. **104**, 221106 (2014).
17. M. S. Minsky, S. B. Fleischer, A. C. Abare, J. E. Bowers, E. L. Hu, S. Keller, and S. P. Denbaars, "Characterization of high-quality InGaN/GaN multiquantum wells with time-resolved photoluminescence," Appl. Phys. Lett. **72**, 1066–1068 (1998).
18. J. W. Shi, J. K. Sheu, C. H. Chen, G. R. Lin, and W. C. Lai, "High-speed GaN-based green light-emitting diodes with partially n-doped active layers and current-confined apertures," IEEE Electron Device Lett. **29**, 158–160 (2008).
19. M. S. Islim, R. X. Ferreira, X. Y. He, E. Y. Xie, S. Videv, S. Viola, S. Watson, N. Bamiedakis, R. V. Penty, I. H. White, A. E. Kelly, E. D. Gu, H. Haas, and M. D. Dawson, "Towards 10 Gb/s orthogonal frequency division multiplexing-based visible light communication using a GaN violet micro-LEDP," Photon. Res. **5**, A35 (2017).
20. J. H. Lau, "Overview and outlook of through-silicon via (TSV) and 3D integrations," Microelectron. Int. **28**, 8–22 (2011).